Pathway Controlled Morphology Formation in Polymer Systems: Reactions, Shear, and Microphase Separation

N. M. Maurits,† G. J. A. Sevink,* A. V. Zvelindovsky,* and J. G. E. M. Fraaije

University of Groningen, Faculty of Mathematics and Natural Sciences, Nijenborgh 4, 9747 AG Groningen, The Netherlands

Received March 5, 1999; Revised Manuscript Received July 7, 1999

ABSTRACT: We present a reactive dynamic mean-field density functional method that gives insight in pathway controlled morphology formation in irreversibly reacting polymer systems that undergo simultaneous micro- and/or macrophase separation. Taking reactive blending as an example for simulations, we show that this type of polymer processing is very effective in emulsifying incompatible polymers and that reactions are essential in obtaining a regularly emulsified blend. Moreover, we show that a rationally designed processing pathway that includes shearing, reactions, and microphase separation can lead to layered structures, and we propose a physical mechanism for this phenomenon.

It is known that many polymer material properties are determined by mesoscale structures, which are typically of the order of 1−1000 nm. The mesoscale morphology is pathway controlled: the morphology is the result of a dynamic balance of factors in which both processing conditions (such as presence of shearing, mixing, extruding, molding, and reactions) and component properties (such as compressibility, miscibility, molecular weight, polydispersity, and polymer stoichiometry) play an important role. A typical example from industrial practice is high-impact polystyrene (HIPS). HIPS is produced via the polymerization of styrene containing dissolved polybutadiene and is a typical product by process, whose morphology results from the in-situ character of (grafting) reactions and from the process technology.[1]

To gain insight into the pathway controlled formation mechanism of mesoscale morphologies such as those found in HIPS and also in composite polymer membranes, latexes formed by emulsion polymerization, and biological cell organelles, it is clearly essential to account for both microphase separation and *irreversible* reaction kinetics in a model. Another example is given by reactive blending, which is one of the simplest industrially interesting problems in which the morphology is pathway controlled. Reactive blending is a very versatile method of strengthening and emulsifying incompatible polymer blends. The technique involves melt blending two homopolymers (A and B) with a fraction of functional reactive groups. If the A-reactive groups are designed to couple with B-reactive groups, the reaction will be confined to interfaces between phases. The product is a graft or block copolymer and is located where it is most effective. The need for dispersing a copolymer surfactant is hence eliminated. Since the mesoscale structures that are formed in these complex systems are the result of *dynamic* processes, they are irregularly structured, full of defects, and very often frozen in a state far from thermodynamic equilibrium. The standard approach to determine polymer phase diagrams of ordered structures at equilibrium by solving a set of self-consistent field equations for a *presupposed* structure of ideal symmetry (see e.g. ref 2) fails to describe the irregular structures in complex polymer fluids. To gain insight into the formation mechanism of irregular morphologies, they should be studied as the dynamic result of diffusive, reactive, and viscoelastic phenomena.

Predictive models for polymer reaction engineering are usually based on kinetic models[3] and do not provide insight into the morphology formation mechanism. Another class of reaction−diffusion models finds many applications in biology as a means to explain morphogenesis by the appearance of spatiotemporal patterns.[4−8] The only available studies on models that combine reactions and phase separation in polymers have mostly focused on chemically reactive binary mixtures and macrophase separation. Most studies employ a Cahn−Hilliard theory of (macro)phase separation that is extended to account for reactions, combined with a Ginzburg−Landau−Wilson free energy. Numerical solutions are obtained by either Monte Carlo methods[9,10] or finite differences.[11−13] The influence of different forward and backward reaction rates and switching on the reaction from the beginning or at a later stage in the spinodal decomposition process have also been studied[12,13] as a means to stabilize and tune the steady-state morphology of phase separating materials. It was also found that the evolution morphology depends critically on the relative time scales of segregation (diffusion) and chemical reaction.[11]

More realistic reaction−diffusion systems with irreversible reactions that can be compared to polymerizing systems are described by Schulz[14,15] in the context of interpenetrating polymer networks (IPN's). In ref 15 the authors focus on (irreversible) homopolymerization of two species and simultaneous (freezing of) spinodal decomposition, which can be described by the usual free energy of a homopolymer mixture.[16] The authors show that the same reactions that initially cause the spinodal decomposition will eventually freeze the SD process. This shows that the presence of irreversible chemical reactions has a strong effect on the evolution of the

† Present address: Groningen University Hospital, Department of Neurology, P.O. Box 30001, 9700 RB Groningen, The Netherlands.

* Corresponding author.

10.1021/ma990336x CCC: $18.00
Published on Web 10/13/1999

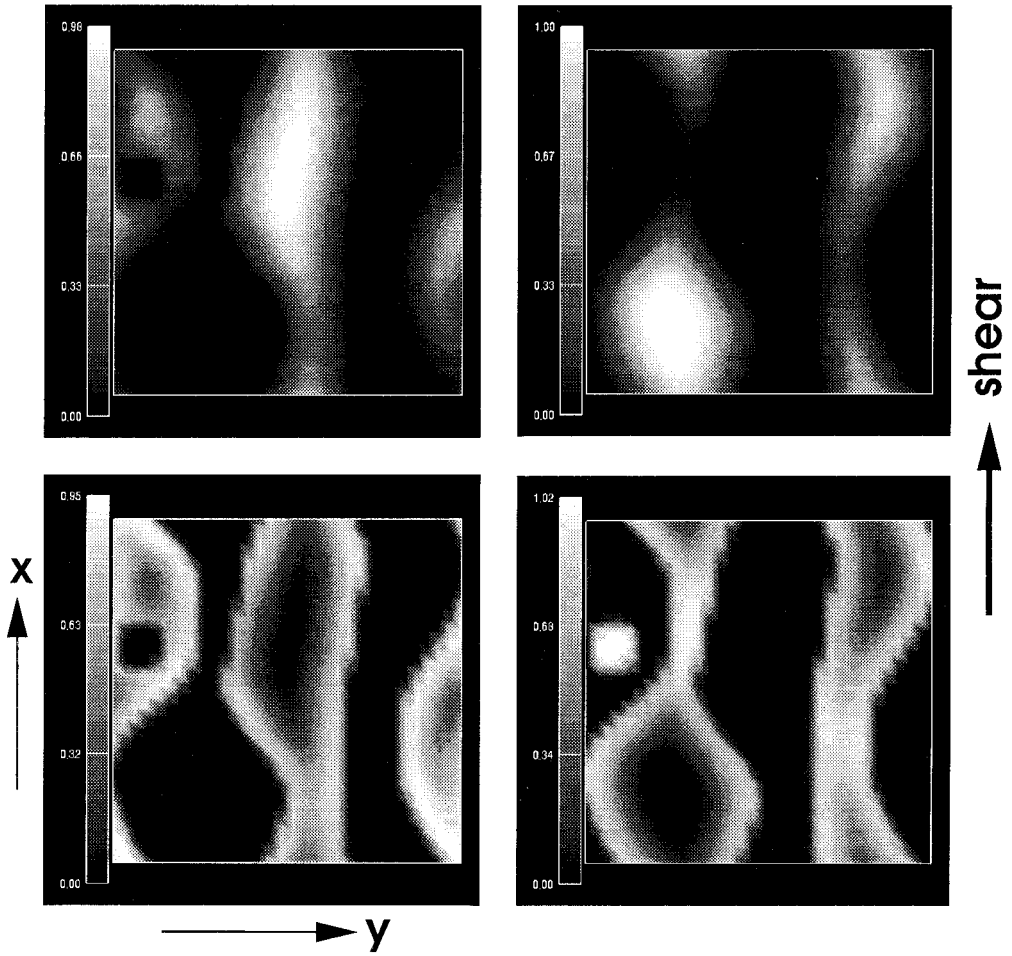

Figure 1. Two-dimensional simulation of a homopolymer blend 50%/50% A_8/B_8. Before the reactions were switched on, 50 000 steps of shear were performed ($\Delta t\dot{\gamma} = 0.001$) on the blend. The shear was stopped at time step 50 000, and subsequently 5000 reaction steps were performed ($\Delta tk/\nu = 0.1$). In the figures the densities of ρ_{hA}, ρ_{hB}, ρ_{dA}, and ρ_{dB} are depicted at time step 55 000 from top left to bottom right. The total volume fractions at this time level are 18.5% A_8, 18.5% B_8, and 63% A_8B_8. High concentration, white; low concentration, black. The arrow indicates the shear direction.

spinodal decomposition process. In ref 14 a mixture of A, B, and irreversibly connected A−B molecules is studied. To describe both micro- and macrophase separation at the same time, the authors show that it is necessary to adapt the Ginzburg−Landau−Wilson Hamiltonian.[17] This Hamiltonian is only valid for very concentrated A−B melts. Especially for very small concentrations A−B, the description is not valid because few molecules A−B can no longer realize stability of microphase separated solutions, and a macrophase separation occurs. This cannot happen according to the GLW Hamiltonian description,[14] because there is always a finite elastic force present.

In this paper we show that by extending the dynamic mean-field density functional theory[18,19] with reactions, the above problem can be resolved, and the formation mechanism of irregular polymer morphologies as the dynamic result of diffusive, reactive, and viscoelastic phenomena can be studied as a function of time. The concentration of polymers in the melt must also be sufficiently high to allow for a mean-field description, but fortunately, the polymers may be of different type, such as homopolymers and/or copolymers, as long as the total concentration of polymer is sufficiently high. This method is therefore, to our knowledge, the first that gives insight into pathway controlled morphology formation in irreversibly reacting polymer systems that undergo simultaneous micro- and/or macrophase separation. Taking reactive blending as an example, we show that this type of polymer processing, as is experimentally known,[20] is very effective in emulsifying incompatible polymers and that reactions are essential in obtaining a regularly emulsified blend. Moreover, we show that a rationally designed processing pathway that includes shearing, reactions, and microphase separation can lead to layered structures, and we propose a physical mechanism for this phenomenon.

The dynamic mean-field density functional theory[18,19] models the behavior of complex liquids by combining Gaussian mean-field statistics with a coarse-grained Ginzburg−Landau model for time evolution of conserved order parameters. In contrast to traditional phenomenological free energy expansion methods,[21−23] the free energy is not truncated at a certain level. Instead, the full polymer path integral is retained by employing numerical algorithms.[19,24,25] Although the repeated calculation of the polymer path integral is computationally very intensive, this approach allows for a description of the mesoscopic dynamics of *specific* complex liquids without constantly adjusting the parameters.[26]

In the dynamic mean-field density functional approach a polymer solution is modeled as a compressible system of ideal Gaussian chain molecules. The free energy functional is derived on the basis of principles from thermodynamics and statistical mechanics and consists of an internal energy term (the ensemble

average of the intrachain Hamiltonian), an entropy term (the ensemble average of ln Ψ where Ψ is the configurational distribution function), and interchain interaction terms. Assuming that the system can be observed on a coarse-grained time scale such that the distribution function is always optimal and hence the free energy always minimal, the free energy functional is then optimized over all Ψ under the constraint that the density that is observed in the system is the ensemble average of a microscopic density operator. The optimal *single*-chain configurational distribution function for a Gaussian chain Hamiltonian is then derived to be[19]

$$\psi = \frac{1}{\phi}\exp(-3/(2a^2)\sum_{s=2}^{N}(\mathbf{R}_s-\mathbf{R}_{s-1})^2-\beta\sum_{s'=1}^{N}U_s(\mathbf{R}_s)) \quad (1)$$

where ϕ is the intramolecular partition function, a is the Gaussian bond length parameter, $\beta^{-1} = k_B T$ with k_B the Boltzmann constant and T the temperature, and N is the number of beads in the chain. The external potentials U_I are conjugate to the density fields ρ_I via the Gaussian chain density functional (the ensemble average, weighted with ψ) and are introduced in the optimization of the free energy under constraint as Lagrange multiplier fields. Path integral calculations are required in the numerical process to calculate the instantaneous density field from a given external potential field. The free energy functional is then derived to be[19,25]

$$F[\{\rho_I\}] = -\frac{1}{\beta}\sum_p \ln\frac{\phi_p^{n_p}}{n_p!} - \sum_I\int_V U_I(\mathbf{r})\,\rho_I(\mathbf{r})\,d\mathbf{r} + \frac{1}{2}\sum_{IJ}\int_{V^2}\epsilon_{IJ}(|\mathbf{r}-\mathbf{r}'|)\rho_I(\mathbf{r})\,\rho_J(\mathbf{r}')\,d\mathbf{r}\,d\mathbf{r}' + \frac{\kappa_H}{2}\int_V(\sum_I \nu_I(\rho_I(\mathbf{r})-\rho_I^0))^2\,d\mathbf{r} \quad (2)$$

where n_I is the number of polymer molecules of species I, ϕ_p is the intramolecular partition function of polymer species p, p is a polymer index, I is a component index, and V is the system volume. The average density is ρ_I^0, and ν_I is the bead volume. The cohesive interactions between chains have kernels $\epsilon_{IJ} \propto \epsilon_{IJ}^0 \exp[-3/(2a^2)(\mathbf{r}-\mathbf{r}')^2]$ where ϵ_{IJ}^0 is a constant interaction parameter and κ_H is the Helfand compressibility parameter.[25] The external potentials U_I are conjugate to the density fields ρ_I via the Gaussian chain density functional.[19]

In dynamic mean-field density functional theory, the dynamics of the polymer melt under simple steady shear is described by the time evolution of density fields ρ_I. The dynamics is governed by a diffusion−convection equation with local kinetic coupling coefficients and sheared periodic boundary conditions[27,28] and can readily be extended with (second order) reaction terms in the following manner:

$$\frac{\partial\rho_I}{\partial t} = M\nabla\cdot\rho_I\nabla\frac{\delta F}{\delta\rho_I} - \dot\gamma y\nabla_x\rho_I + \sum_{J=1,K=1}^{N} k_{JK}\rho_J\rho_K + \eta_I \quad (3)$$

Here M is a mobility parameter. The velocity field for simple steady shear is given by $v_x = \dot\gamma y$ where $\dot\gamma$ is the shear rate. If no shear is applied, $\dot\gamma = 0$. η_I is a stochastic term which is distributed according to a fluctuation−dissipation theorem,[29] and k_{JK} is the reaction rate which can be either negative for reactants or positive for products. Notice that the reactive noise can be neglected here.[30] Different order reactions or multiple reaction terms can be added without any difficulties, but as a proof of principle, we focus here on the above type of reactions. It is possible to introduce more advanced nonlocal Rouse or reptation models for the kinetic coefficients.[31] In the present paper we study the effect of combined microphase separation, shear *and* reaction, to gain insight into the mechanisms that are important in pathway controlled morphology formation and in particular in reactive blending. In general, hydrodynamic and viscoelastic phenomena are also of interest in simulations of polymer morphology formation, and their separate effect was studied by our group in refs 32 and 33. To make a true evaluation of reactive effects in a model that can account for both micro- and macrophase separation, we have chosen not to include hydrodynamic and viscoelastic effects. Given our results in refs 32 and 33, we do not expect these effects to be of great influence in the chosen simulation environment.

Since we focus on reactive blending, we study a reaction in which a homopolymer A_8 couples to a homopolymer B_8 to form a diblock copolymer A_8B_8. The reaction is limited to the end groups, and we assume that if two blocks that can couple are close enough, the reaction takes place. This reaction can be modeled as follows:

$$\frac{\partial\rho_{hA}}{\partial t} = M\nabla\cdot\rho_{hA}\nabla\frac{\delta F}{\delta\rho_{hA}} - \dot\gamma y\nabla_x\rho_{hA} - k\rho_{hA}\rho_{hB} + \eta_{hA} \quad (4a)$$

$$\frac{\partial\rho_{hB}}{\partial t} = M\nabla\cdot\rho_{hB}\nabla\frac{\delta F}{\delta\rho_{hB}} - \dot\gamma y\nabla_x\rho_{hB} - k\rho_{hA}\rho_{hB} + \eta_{hB} \quad (4b)$$

$$\frac{\partial\rho_{dA}}{\partial t} = M\nabla\cdot\rho_{dA}\nabla\frac{\delta F}{\delta\rho_{dA}} - \dot\gamma y\nabla_x\rho_{dA} + k\rho_{hA}\rho_{hB} + \eta_{dA} \quad (4c)$$

$$\frac{\partial\rho_{dB}}{\partial t} = M\nabla\cdot\rho_{dB}\nabla\frac{\delta F}{\delta\rho_{dB}} - \dot\gamma y\nabla_x\rho_{dB} + k\rho_{hA}\rho_{hB} + \eta_{dB} \quad (4d)$$

Here, ρ_{hA}/ρ_{hB} is the density of A/B beads in the homopolymer, ρ_{dA}/ρ_{dB} is the density of A/B beads in the diblock copolymer, and k is the reaction rate of the coupling reaction.

We have performed a number of simulations in 2D according to eq 3 to enhance our understanding of the important mechanisms in the pathway controlled morphology formation in reactive blending. Details of our numerical integration schemes are in ref 19. We study a model system that provides insight in the main features of reactive blending. Our method may be used as an engineering tool for a specific system. A blend of 50% A_8 and 50% B_8 was sheared ($\Delta t\dot\gamma = 0.001$, $\Delta\tau = Dh^{-2}\Delta t$, h is the grid size with $a/h = 1.15430$) for 50000 dimensionless time steps on a 32×32 grid until the system had relaxed. The value of the shear rate is chosen such that it represents an experimentally real-

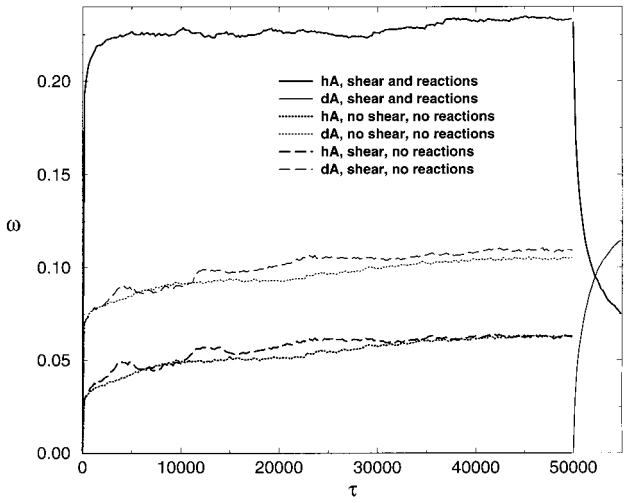

Figure 2. Dimensionless order parameter ω as a function of dimensionless time step τ.

istic value. The dimensionless interaction parameters are $\beta\epsilon_{IJ}/\nu = 2.5$ for incompatible species and $\beta\epsilon_{IJ}/\nu = 0$ for compatible species.[19] The reaction that is described earlier was initiated at time step 50 000 and was followed for 5000 time steps ($\Delta tk/\nu = 0.1$). The diffusion coefficient and reaction rate are chosen such that the diffusive and reactive contributions to the dynamic equations are comparable in magnitude (measured by the L^2 norm) at time step 50 000. The results that are depicted in Figure 1 clearly show that the in-situ copolymerization leads to stabilized structures in which the homopolymer domains are shielded from each other by a layer of diblock copolymer. The stabilized structures are large and regular. The dimensionless order parameter $\omega_I \equiv (1/V)\int_V(\theta_I^2(\mathbf{r}) - \theta_{I,0}^2(\mathbf{r}))\,d\mathbf{r}$, where $\theta_I = \nu\rho_I$ is the dimensionless density and subscript 0 denotes average values, is shown for both ρ_{hA} and ρ_{dA} in Figure 2 (drawn lines). The effect of the reactions that are switched on at time step 50 000 is clearly visible: the order parameter of the homopolymer decays exponentially whereas the order parameter of the diblock increases at the same time by the same amount. To check the influence of the assumption that two blocks can couple if they are close enough, we have run two simulations in 2D (results not shown) on a 32×32 grid. A homogeneously mixed 40%/60% A_8/B_8 blend was allowed to relax for 500 dimensionless time steps, after which reactions were switched on for 500 dimensionless time steps ($\Delta tk/\nu = 0.1$). We compared the results for a run in which reaction only takes place if two A and B *end* beads are close enough to a run in which the reaction takes place if the two blocks are close enough. As expected, this only influences the time scale of the reactions: the reactions are found to be faster by a factor $2.8 \sim \sqrt{N}$ if the end beads are not explicitly distin-

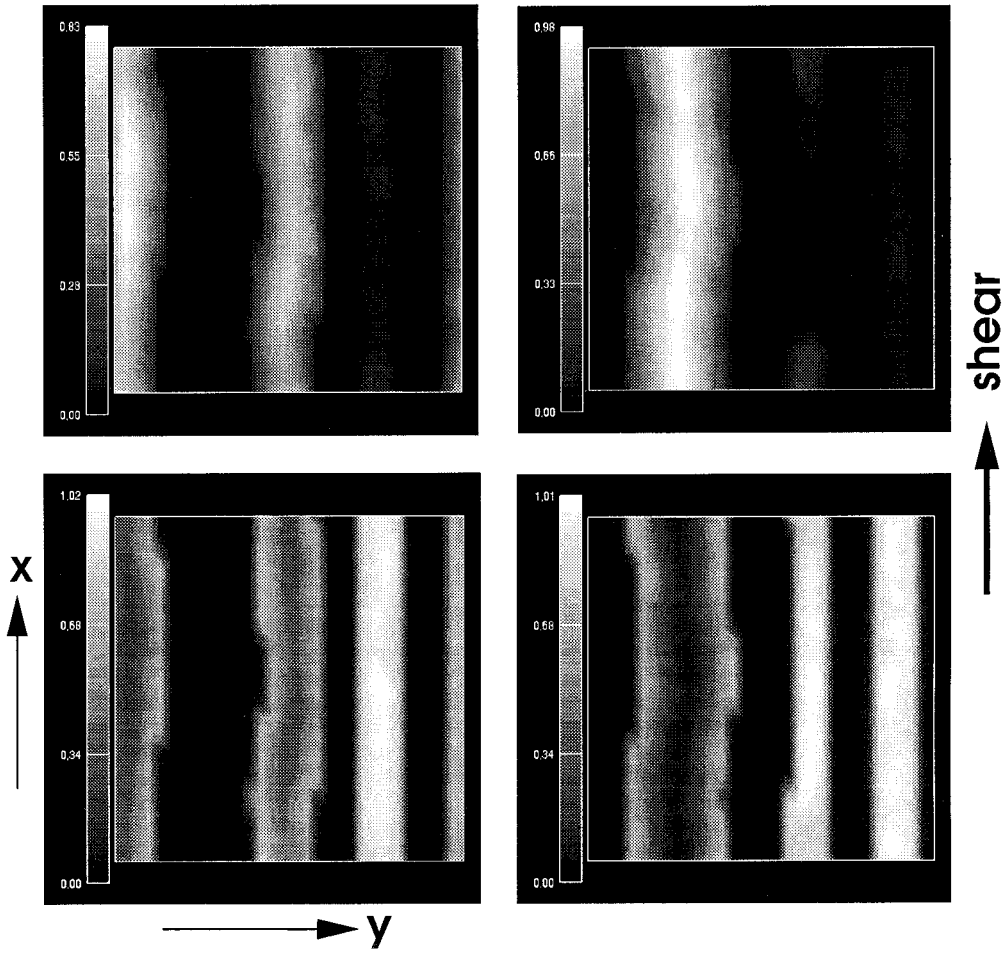

Figure 3. Two-dimensional simulation of a homopolymer/diblock copolymer mixture with 18.5% A_8, 18.5% B_8, and 63% A_8B_8. The initial system is homogeneously mixed. Shear was applied for 50 000 time steps on the (micro/macro)phase separating mixture ($\Delta t\dot{\gamma} = 0.001$). In the figures the densities of ρ_{hA}, ρ_{hB}, ρ_{dA}, and ρ_{dB} are depicted at time step 50 000 from top left to bottom right. The total volume fraction of each species is constant during this simulation. High concentration, white; low concentration, black. Same shear direction as in Figure 1.

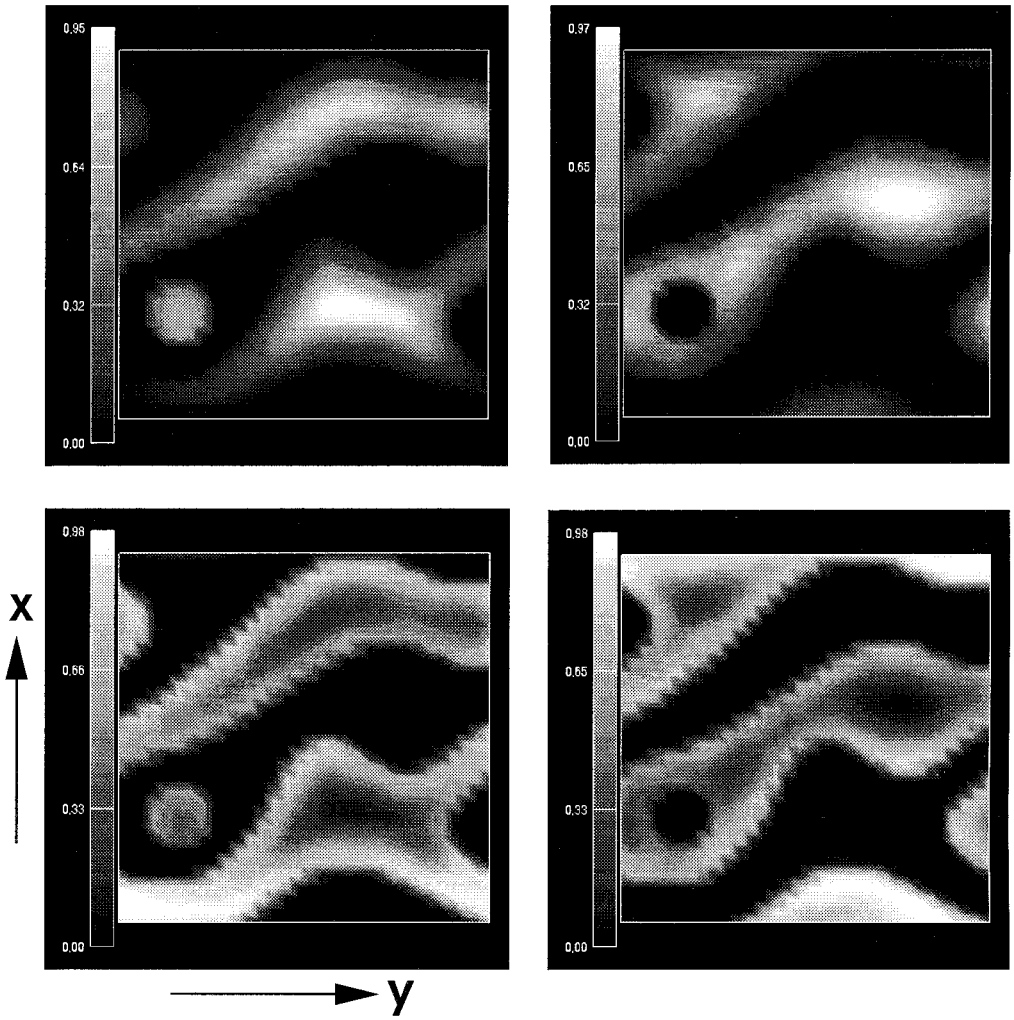

Figure 4. Two-dimensional simulation of a homopolymer/diblock copolymer mixture with 18.5% A_8, 18.5% B_8, and 63% A_8B_8. The initial system is homogeneously mixed. The system is (micro/macro)phase separating for 50 000 time steps. No additional shear is applied. In the figures the densities of ρ_{hA}, ρ_{hB}, ρ_{dA}, and ρ_{dB} are depicted at time step 50 000 from top left to bottom right. The total volume fraction of each species is constant during this simulation. High concentration, white; low concentration, black.

guished. These results comply nicely with the result by Fredrickson[34] that the reaction rate for diffusion controlled reactions in polymers is proportional to the radius of gyration.

As a comparison and to establish the importance of the particular pathway that we chose for reactive blending, we have also performed two simulations using the same parameters starting from a homogeneous mixture of the same concentrations of homopolymer/copolymer as in the reactive run at time step 55 000 (18.5% A_8, 18.5% B_8, and 63% A_8B_8). The purpose of these runs is to see whether blending can be as effective without reactions. The first simulation (see Figure 3) consists of 50 000 time steps of shear ($\Delta t\dot{\gamma} = 0.001$) on the initially homogeneous homopolymer/copolymer mixture. The results in Figure 3 show the final morphology at time step 50 000. The most striking difference with the reactive run is that the phases are unevenly distributed because of macrophase separation. The diblock copolymer is concentrated in the right half of the box, and the homopolymer is concentrated in the left half. Only a very small amount of diblock copolymer is effective in shielding the two types of homopolymer from each other. The macrophase separation in the presence of diblock copolymers is probably due to the high concentration of diblock copolymer compared to the monomer concentrations. If there is no incentive to form droplets (as result form the sheared blend in Figure 1), it is more effective to form "stripes" of monomer in a sheared periodic system which require less diblock copolymer to be shielded from each other. The excess diblock copolymer then forms layers by itself. In the system in Figure 1, reactions take place so fast that monomer does not diffuse through the diblock copolymer layer anymore, and no macrophase separation takes place.

The second simulation (see Figure 4) consists of 50 000 time steps of (micro/macro)phase separation dynamics only on the initially homogeneous homopolymer/copolymer mixture. The results in Figure 4 show the final morphology at time step 50 000. Although at first sight the results do not seem much different from the reactive run, close observation shows that the homopolymer domains are not as effectively shielded from each other as in the reactive run. The diblock copolymer layer is either less pronounced, or the diblock copolymers form domains by themselves (lower part of the box). This conclusion is backed up by the structure factors of both systems (results not shown). The structure factor of the A beads in the diblock in the first 2D run shows a peak that is larger and more localized than in the third 2D run. Moreover, the order parameters of

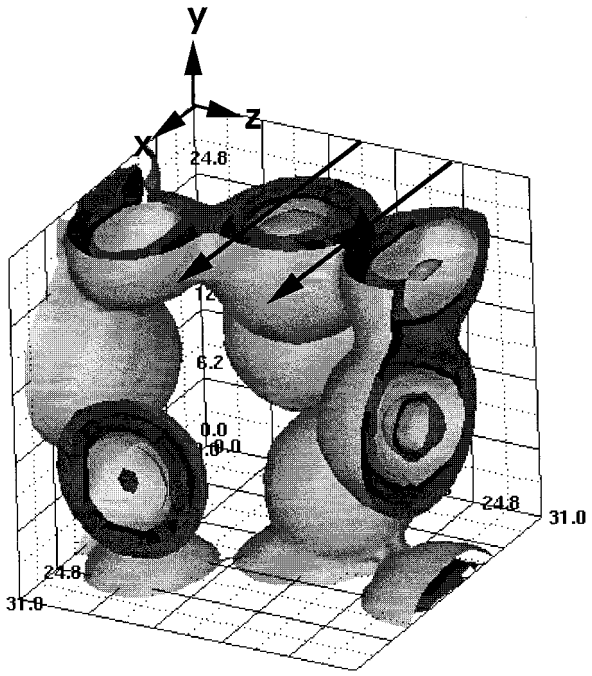

Figure 5. Three-dimensional simulation of a homopolymer blend 90%/10% A_8/B_8. Before the reactions were switched on, 28 000 steps of shear were performed ($\Delta t\dot{\gamma} = 0.001$) on the blend. The shear was stopped at time step 28 000, and 2500 reaction steps were performed ($\Delta tk/\nu = 0.1$). In the figure the isodensity surfaces at different levels are depicted at time step 30 500 of ρ_{hB}, ρ_{dA}, and ρ_{dB}. The total volume fractions at this time level are 80.5% A_8, 0.5% B_8, and 19% A_8B_8. The arrows indicate the shear direction.

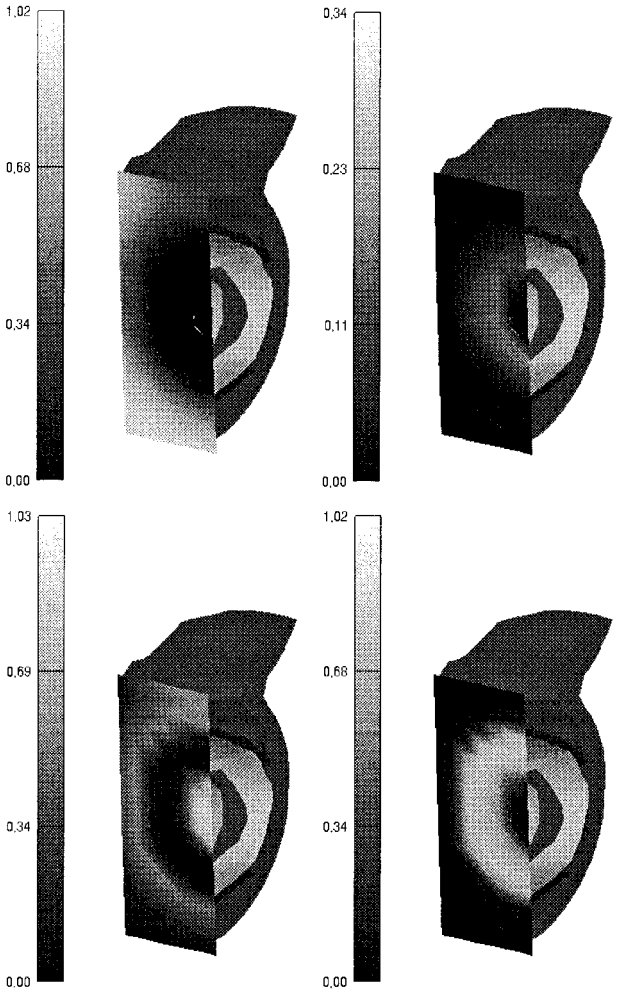

Figure 6. Detail of Figure 5. From top left to bottom right the densities of ρ_{hA}, ρ_{hB}, ρ_{dA}, and ρ_{dB} are depicted in the slices at time step 30 500. High concentration, white; low concentration, black.

all 2D runs show that the ordering of both the homopolymer and the diblock copolymer in the reactive run is higher than in the nonreactive runs (see Figure 2, dashed and dotted lines) for the fully relaxed systems. We conclude, as is found in experiments,[20] that reactive blending is very effective in emulsifying incompatible polymer blends and that reactions are essential in obtaining a regularly emulsified blend. Moreover, the resulting morphology is sensitively dependent on the chosen pathway. The blend should be sheared for a substantial period of time before reactions set in. We have also performed simulations in which the reactions set in immediately, with and without applied shear (results not shown), which yields irregular lamellar structures (since the homopolymer almost completely reacts) that are considerably smaller in size.

Finally, we have performed a three-dimensional simulation of reactive blending. A 90%/10% A_8/B_8 homopolymer blend was sheared in a $32 \times 32 \times 32$ box for 28 000 dimensionless time steps until the system had relaxed ($\Delta t\dot{\gamma} = 0.001$). All other simulation parameters are the same as in the 2D systems. The reaction that is described earlier was initiated at time step 28 000 and was followed for 2500 time steps ($\Delta tk/\nu = 0.1$). Figures 5 and 6 show some results at time step 30 500. Again, the results show that reactive blending is very effective in emulsifying incompatible polymer blends. A very exciting result is that we observe the formation of layered structures for the first time. Some of the droplets that were originally present in the relaxed blend also contain a diblock copolymer micelle on the *inside* after reactions. To gain more insight into the formation of these structures, we have plotted a few snapshots of isoslices of the A part of the diblock copolymer at different time steps in one of the layered structures in Figure 7. This shows that the total amount of diblock copolymer increases inside the initial droplet. The amount of diblock copolymer on the interface is increasing as long as there is enough B monomer present to keep the reaction going. In a later stage of the simulation further diffusion has caused the elongated structure to become more spherical. If the initial droplet is too small (see Figure 8), the diblock copolymer that is initially present inside the droplet may diffuse to the outside again if the structure has become more spherical and the concentration of diblock copolymer is too low to form a stable micellar structure inside. We propose the following mechanism for formation of these layered structures (see Figure 9). Since the original blend is sheared, the resulting droplets are elongated (see Figure 10). Once the reactions start and shear is stopped, two mechanisms are taking place at the same time: due to the reactions diblock copolymer is formed at the homopolymer interface, and due to relaxation mechanisms the elongated droplet relaxes to a sherical shape. The surface of the elongated droplet is larger than the surface of the spherical droplet with the same volume, so that the fast reactions lead to an excess of diblock copolymer at the interface. This excess copolymer can be transported to the inside of the droplet to

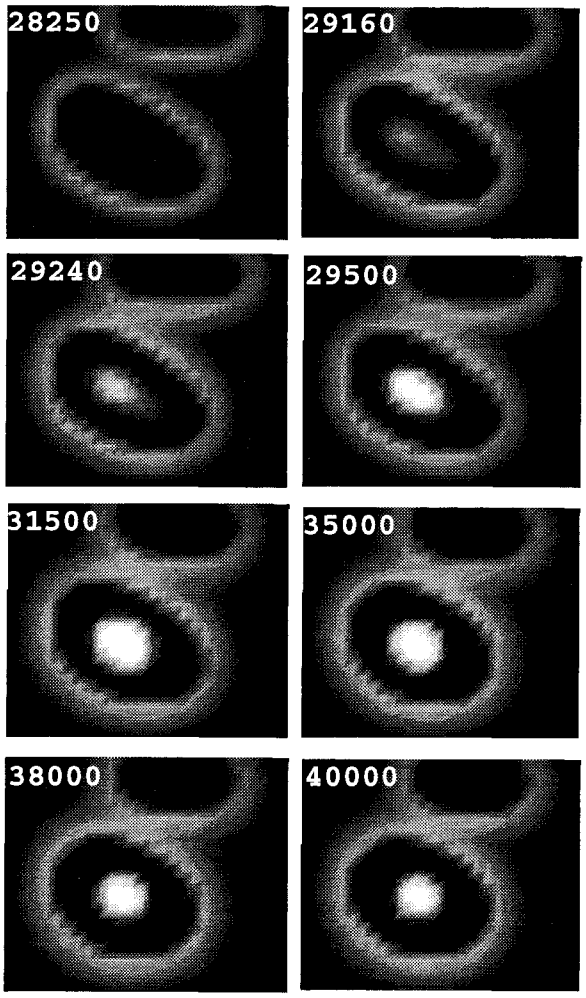

Figure 7. Detail of Figure 5. Snapshots of a slice through a large bubble (densities of ρ_{dA}) at different time steps: 28 250, 29 160, 29 240, 29 500, 31 500, 35 000, 38 000, and 40 000. Although the slicing direction is different, the bubble is the same as shown in Figure 6. High concentration, white; low concentration, black.

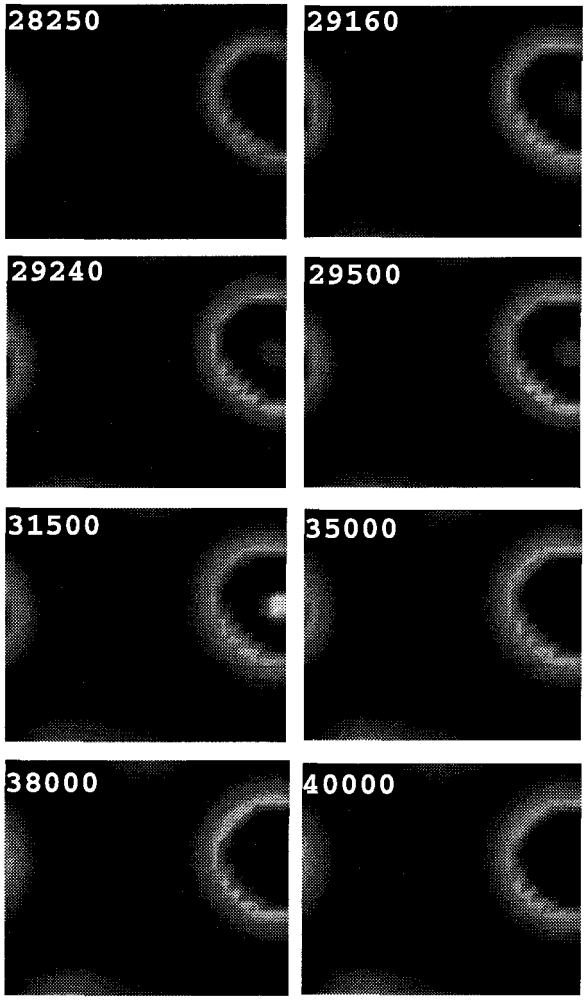

Figure 8. Detail of Figure 5. Snapshots at the same time steps as in Figure 7 at a different slicing position in the simulation box, following the time evolution of a smaller bubble (densities of ρ_{dA}). High concentration, white; low concentration, black.

form a micellar shape, or it can be transported to outside the droplet. In the case of a symmetric diblock copolymer this latter option is energetically less favorable at low concentrations because formation of flat layers is impossible. This simulation clearly indicates a possible method to obtain layered structures from reactive blending processes. The formation of these phases appears to be very sensitive to the balance between reactive and diffusive time scales. The proposed mechanism indicates that it must be possible to rationally design a *multi*layered structure by a delicate balance of shear, reactions, and microphase separation (e.g., higher shear and slightly slower reactions). This will be the subject of future research.

As a comparison, we have also simulated the dynamics of a homogeneous mixture of 80.5% A_8, 0.5% B_8, and 19% A_8B_8 in a 3D 32 × 32 × 32 box (end concentrations reactive run) using the same parameters as in the reactive 3D simulation. Without reactions and without application of shear, we find that the diblock copolymer forms simple micelles in the A_8 homopolymer matrix in which the B block is protected from unfavorable contacts by the A block. We do not observe any formation of layered structures in this simulation (see Figure 11 and cf. Figure 6, bottom left).

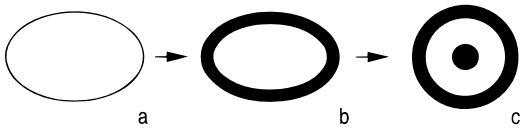

Figure 9. Proposed mechanism for layered structure formation. Diblock (dark) is formed at the interface of the homopolymer droplet (light) (a and b). Two mechanisms take place at the same time (microphase separation and reactions), and excess diblock is transported to the inside to form a layered structure instead of a simple micelle (c).

Conclusion

We have shown that a reactive dynamic mean-field density functional method can give insight by simulation in pathway controlled morphology formation in irreversibly reacting polymer systems that undergo simultaneous micro- and/or macrophase separation. Taking reactive blending as an example, we have shown that we can reproduce the experimentally found effectiveness of this type of polymer processing in emulsifying incompatible polymers. Within the context of the model, our results show that reactions are essential in obtaining a regularly emulsified blend. Moreover, we show that a rationally designed processing pathway that includes a delicate balance of shearing, reactions, and microphase separation can lead to rarely observed

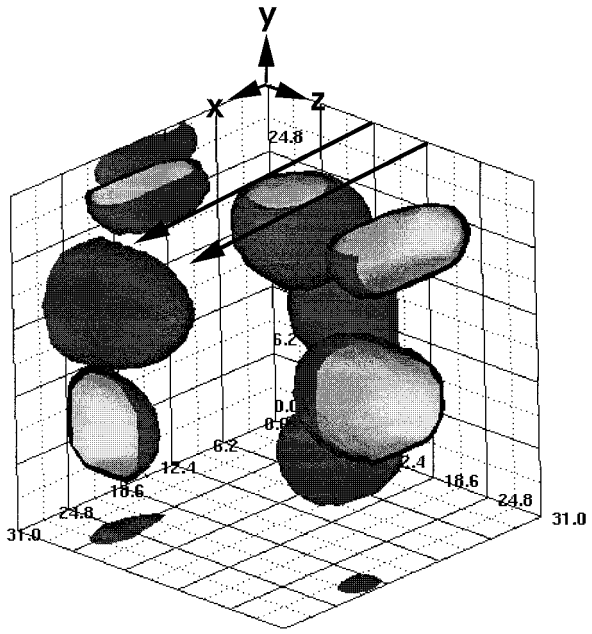

Figure 10. Three-dimensional simulation of a sheared ($\Delta t\dot{\gamma} = 0.001$) homopolymer blend 90%/10% A_8/B_8. Isodensity surfaces at different levels are shown at time step 28 000 of ρ_{hA} and ρ_{hB}. The elongation of the droplets due to the shear is clearly visible.

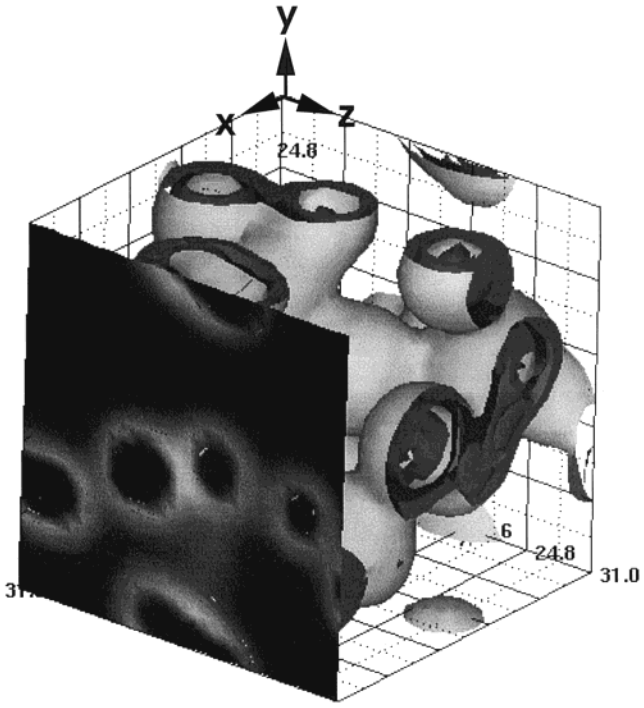

Figure 11. Three-dimensional simulation of a homogeneous mixture of 80.5% A_8, 0.5% B_8, and 19% A_8B_8. Isodensity surfaces at different levels are shown at time step 4500 of ρ_{hA}, ρ_{dA}, and ρ_{dB}. The density of ρ_{dA} is depicted in the slice for further clarification. High concentration, white; low concentration, black.

layered structures, and we propose a physical mechanism for this phenomenon.

Acknowledgment. N.M.M., G.J.A.S., and A.V.Z. acknowledge the support of the ESPRIT project MESODYN No. EP 22685 of the European Commission. We thank A. Morozov for providing some of the data.

References and Notes

(1) Fischer, M.; Hellmann, G. *Macromolecules* **1996**, *29*, 2498−2509.
(2) Leibler, L. *Macromolecules* **1980**, *13*, 1602−1617.
(3) Gilbert, R. G. *Emulsion Polymerization—A Mechanistic Approach*; Academic Press: London, 1995.
(4) Turing, A. *Philos. Trans. R. Soc. London, Ser. B* **1952**, *237*, 37.
(5) Prigogine, I.; Nicolis, G. *J. Chem. Phys.* **1967**, *46*, 3542.
(6) Huberman, B. A. *J. Chem. Phys.* **1976**, *65*, 2013−2019.
(7) Pearson, J. E. *Science* **1993**, *261*, 189−192.
(8) Cross, M.; Hohenberg, P. *Science* **1994**, *263*, 1569.
(9) Glotzer, S. C.; Stauffer, D.; Jan, N. *Phys. Rev. Lett.* **1994**, *72*, 4109−4112.
(10) Glotzer, S. C.; Marzio, E. A. D.; Muthukumar, M. *Phys. Rev. Lett.* **1995**, *74*, 2034−2037.
(11) Puri, S.; Frisch, H. L. J. *Physics A* **1994**, *27*, 6027−6030.
(12) Christensen, J. J.; Elder, K.; Fogedby, H. C. *Phys. Rev. E* **1996**, *54*, R2212−R2215.
(13) Motoyama, M. *J. Phys. Soc. Jpn.* **1996**, *65*, 1894−1897.
(14) Schulz, M.; Frisch, H. L. J. *Chem. Phys.* **1994**, *101*, 5013−5016.
(15) Schulz, M.; Paul, B. *Phys. Rev. B* **1998**, *58*, 11096−11098.
(16) de Gennes, P.-G. *Scaling Concepts in Polymer Physics*; Cornell University; Ithaca, NY, 1979.
(17) de Gennes, P.-G. *J. Phys. Lett.* **1979**, *40*, 69.
(18) Fraaije, J. G. E. M. *J. Chem. Phys.* **1993**, *99*, 9202−9212.
(19) Fraaije, J. G. E. M.; van Vlimmeren, B. A. C.; Maurits, N. M.; Postma, M.; Evers, O. A.; Hoffmann, C.; Altevogt, P.; Goldbeck-Wood, G. *J. Chem. Phys.* **1997**, *106*, 4260−4269.
(20) Guégan, P.; Macosko, C. W.; Ishizone, T.; Hirao, A.; Nakahama, S. *Macromolecules* **1994**, *27*, 4993−4997.
(21) Cahn, J. W.; Hilliard, J. E. *J. Chem. Phys.* **1958**, *28*, 258−267.
(22) Oono, Y.; Puri, S. *Phys. Rev. Lett.* **1987**, *58*, 836−839.
(23) de Gennes, P. G. *J. Chem. Phys.* **1980**, *72*, 4756−4763.
(24) Maurits, N. M.; Altevogt, P.; Evers, O. A.; Fraaije, J. G. E. M. *Comput. Polym. Sci.* **1996**, *6*, 1−8.
(25) Maurits, N. M.; van Vlimmeren, B. A. C.; Fraaije, J. G. E. M. *Phys. Rev. E* **1997**, *56*, 816−825.
(26) van Vlimmeren, B. A. C.; Maurits, N. M.; Zvelindovsky, A. V.; Sevink, G. J. A.; Fraaije, J. G. E. M. *Macromolecules* **1999**, *32*, 6446−6456.
(27) Zvelindovsky, A. V.; Sevink, G. J. A.; van Vlimmeren, B. A. C.; Maurits, N. M.; Fraaije, J. G. E. M. *Phys. Rev. E* **1998**, *57*, R4699.
(28) Zvelindovsky, A. V.; van Vlimmeren, B. A. C.; Sevink, G. J. A.; Maurits, N. M.; Fraaije, J. G. E. M. *J. Chem. Phys.* **1998**, *109*, 8751−8754.
(29) van Vlimmeren, B. A. C.; Fraaije, J. G. E. M. *Comput. Phys. Commun.* **1996**, *99*, 21−28.
(30) Keizer, J. *Statistical Thermodynamics of Nonequilibrium Processes;* Springer: New York, 1987.
(31) Maurits, N. M.; Fraaije, J. G. E. M. *J. Chem. Phys.* **1999**, *107*, 5879−5889.
(32) Maurits, N. M.; Zvelindovsky, A. V.; Sevink, G. J. A.; van Vlimmeren, B. A. C.; Fraaije, J. G. E. M. *J. Chem. Phys.* **1998**, *108*, 9150−9154.
(33) Maurits, N. M.; Zvelindovsky, A. V.; Fraaije, J. G. E. M. *J. Chem. Phys.* **1998**, *109*, 11032−11042.
(34) Fredrickson, G. H. *NATO Adv. Study Inst. Ser.* **1997**, *339*, 315−330.

MA990336X